

Performance of self-centering steel moment frame considering stress relaxation in prestressed cables

Advances in Structural Engineering
1–10

© The Author(s) 2020

Article reuse guidelines:

sagepub.com/journals-permissions

DOI: 10.1177/1369433219900940

journals.sagepub.com/home/ase



Seyyed Morteza Asadolahi and Nader Fanaie 

Abstract

Buildings can be designed to limit the earthquake-induced damage to members that can easily be repaired. Self-centering moment-resisting frames can be used as effective structural systems for this purpose. Self-centering moment-resisting frames with prestressed cables are able to return the structure to its original position after the earthquake. The internal forces in self-centering moment-resisting frames are transferred between the beam and the column by post-tensioned cables. As a main member of self-centering connections, prestressed cables play a significant role in such systems. Cable tension decreases over time due to the effect of stress relaxation on the performance of the system. Stress relaxation is a time-dependent phenomenon causing stress reduction over time in the members prestressed at a constant strain. Therefore, the effect of stress relaxation on the performance of self-centering moment-resisting frames can be significant. In this article, after simulating and validating a moment-resisting frame with self-centering connections, stiffness and moment–rotation hysteresis diagrams were analyzed after 0, 1, 5, 10, and 20 years of cable prestressing. According to the results, two equations were presented to estimate the reduction in the connection stiffness and dissipated energy by the system based on prestressing level and the time after prestressing. The proposed equations could be used to model semi-rigid connections.

Keywords

connection stiffness, hysteresis curve, moment-resisting frames, prestressed cable, self-centering connection, stress relaxation

Introduction

During Northridge (1994) and Kobe (1995) earthquakes, welded moment-resisting frames (MRFs) that were used as earthquake-resistant systems experienced brittle fractures in beam-to-column connections (Miller, 1998; Nakashima et al., 1995). Thereafter, many studies have been conducted to improve the seismic performance of MRFs by beam–column connections with reduced beam flange and connections reinforced with cover and side plates (Engelhardt and Sabol, 1998; Tremblay and Filiatrault, 1997). Earthquake-induced damage, however, is inevitable in this type of MRFs. Currently, most of the structural systems are designed to tolerate loads beyond the elastic limit, leading to mechanisms in certain zones of the structural system (Filiatrault et al., 2004).

Buildings can be designed in such a way that damages would be limited to repairable members. The structural system with this capability is called self-centering moment-resisting frame (SC-MRF). Such systems show higher resistance against collapse than the conventional MRFs do thanks to additional dampers (Guan et al., 2018; Tzimas et al., 2015). In

self-centering (SC) connections, high-strength post-tensioned cables or rebars are used parallel to the beam web throughout the span of the frame restrained by a clamp anchor on the flange of the outer columns of the frame. The cables can significantly reduce the peak displacement and residual drift of the steel frame structure (Dong et al., 2019; Lafortune et al., 2017). Figure 1 shows an SC-MRF with post-tensioned cables in which a connecting angle is used as an energy damper. Due to the post-tensioning force after earthquake and opening in the connection gap, these post-tensioned cables or rebars tend to return the structure to its original position. The total area of the prestressed cables and the yield strength of the dampers

Faculty of Civil Engineering, K. N. Toosi University of Technology, Tehran, Iran

Corresponding author:

Nader Fanaie, Faculty of Civil Engineering, K. N. Toosi University of Technology, No. 1346, Vali-Asr Street, P.O. Box 15875-4416, 19697 Tehran, Iran.

Email: fanaie@kntu.ac.ir

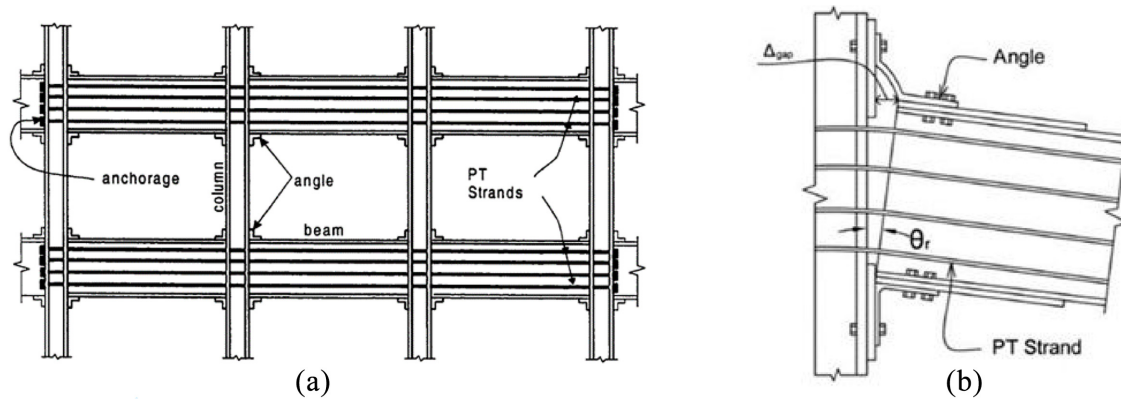


Figure 1. Details of structural elements: (a) seating and top angles of an SC steel frame with post-tensioned cables and (b) an open external connection of the frame (Garlock et al., 2005).

have the greatest influence on the hysteresis behavior of the SC systems (Xian et al., 2017).

These connections comprise energy dissipater devices that experience plastic deformations during cyclic movements of the frame, which dissipate seismic energy. Figure 2 shows the moment–rotation ($M-\theta_r$) response of an SC steel frame where θ_r is the relative rotation between the beam and the column. This flag-shaped behavior is governed by gap opening (Δ_{gap}) and closing of the connection when it is subjected to cyclic loading. Initial stiffness of the connection prior to gap opening is the same as that of a welded

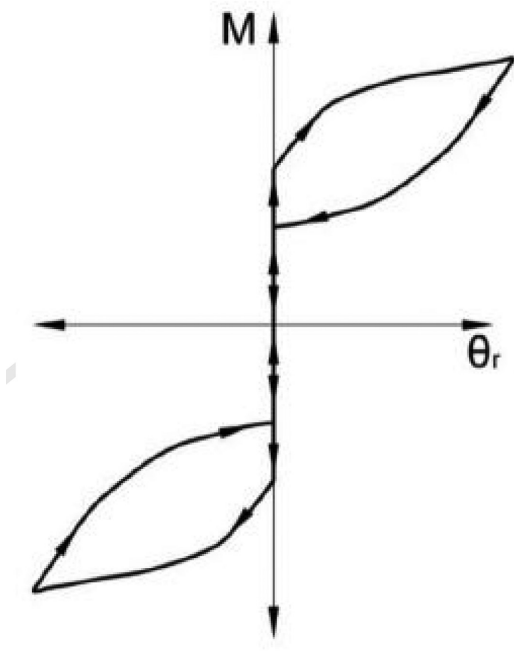


Figure 2. Moment rotation response of an SC connection (Garlock et al., 2005).

connection. However, after the decompression moment (M_d), which initiates the gap opening, it is defined by stiffness of the angle and elastic stiffness of the cables. During loading, the angles yield and, upon unloading, they will dissipate energy (Garlock et al., 2005).

Although SC connections have been proven to be a proper alternative to semi-rigid connections, there are still not much guidelines in the current seismic design codes. Thus, further research studies are required to thoroughly investigate the application of these connections to buildings. In this regard, finite element (FE) analysis is an appropriate method that provides the possibility to analyze the behavior of SC connections. Several FE studies have been carried out in order to investigate the effect of different factors on the performance of existing connections with SC capability (Al Kajbaf et al., 2018).

The behavior of a load-bearing structure is a combination of instantaneous (short-term) and long-term behaviors. The instantaneous structural behavior at the time of loading and its long-term behavior are dependent on material properties and support conditions. Typical long-term structural behaviors include concrete creep and relaxation of prestressed steel. The stiffness of the SC system mainly depends on the initial prestress and stiffness of cables (Huanga et al., 2018; Smith et al., 2014). Prestressed cables as the main members of SC connections are subject to stress relaxation, which is a time-dependent phenomenon occurring when stress is applied to a constant length. Ignoring stress reduction under stress relaxation leads to an inaccurate picture of the local and general behaviors of the structure in the long term. This study is aimed at using the ABAQUS software (ABAQUS/PRE, 2011) to investigate the behavior of an SC connection under stress relaxation over time. To this end, stiffness and

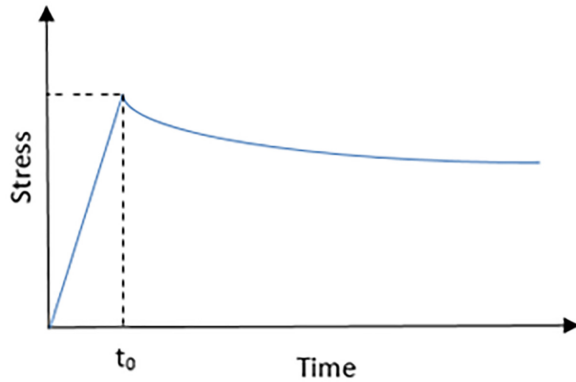


Figure 3. Stress reduction under stress relaxation (Findley et al., 1976).

moment–rotation hysteresis diagrams are examined after 0, 1, 5, 10, and 20 years of cable prestressing under the influence of different prestressing forces.

Stress relaxation

Stress relaxation is defined as the loss of stress when the stressed material is held at a constant length (constant strain; Magura et al., 1964). Reduction in initial prestressing with time is one of the main concerns in the design of prestressed members. Despite the importance of accurate estimation of the ultimate prestressing for design purposes, the determination of this parameter is complicated because of its dependence on time as well as material and environmental characteristics (Sreevalli and Rao, 2010). Factors affecting stress relaxation include prestressing duration, steel type, initial stress, history of re-tensioning, and temperature. Creep in concrete, which is defined as increased deformation at constant stress, is another manifestation of this phenomenon (Magura et al., 1964). Figure 3 schematically displays the effect of stress relaxation on the prestressed cable. As shown in Figure 3, the structure shows an instantaneous response to the load at a very short time, t_0 . The long-term behavior of the structure is observed in a longer time depending on materials and support conditions.

Many studies have been carried out to investigate the dependence of relaxation of steel on these factors (Magura et al., 1964). Trevino and Ghali (1985) presented an equation for the relaxation reduction coefficient and used it in the prestressed concrete design. Zeren and Zeren (2003) investigated the effect of temperature on the relaxation behavior and derived empirical formulas from relaxation test data. Subsequent studies on cable stress relaxation were gradually directed toward the application analysis of stress relaxation in practical structures to investigate

the degradation influence. Au and Si (2012) considered the rheological behavior and conducted a long-term time-dependent analysis of cable-stayed bridges by time integration. Atienza and Elices (2007) performed experimental and numerical studies on stress relaxation losses in steel tendons to reveal the relationship between stress relaxation and residual stress in SWs of prestressed concrete.

Most investigations for estimating stress relaxation do not exceed a duration of one and a half years. Magura et al. (1964) predicted stress relaxation in a prestressed member under different conditions by conducting several tests on a variety of cables. They proposed a logarithmic formula as a function of time change only with the initial prestressing ratio. The following equation is used for calculating residual stress in SC connection

$$\frac{f_s}{f_{si}} = 1 - \frac{\log t}{10} \left(\frac{f_{si}}{f_y} - 0.55 \right) \text{ for } \frac{f_{si}}{f_y} \geq 0.55 \quad (1)$$

where f_s represents the residual stress at any time after prestressing, f_{si} the initial prestressing, f_y the yield stress, and t is the time in hours. This formula has recently been used by Au and Si (2012).

FE modeling of the steel frame with SC connection

A typical SC steel frame experimentally studied by Garlock et al. (2005) was modeled three-dimensionally in the ABAQUS software to investigate the behavior of the SC connection. Garlock et al. (2005) experimentally tested full-scale interior post-tensioned energy dissipating (PTED) connections with bolted top-and-seat angles and high-strength post-tensioned cables under cyclic loading. In this study, since no particular failure mode was considered for the SC connection to take into account the influence of stress relaxation, 36s-20-P specimen was selected, which did not experience any specific failure during the test. The selected specimen had 36 cables and a flange reinforcement plate. The total post-tensioning force of cables was 3194 kN.

Geometry modeling

Figure 4 displays the configuration of the selected specimen. The beam cross section for all samples equaled W36 × 150 with a nominal yield stress (σ_{yn}) of 345 MPa. A reinforcement plate was also welded to the beam flanges. The column cross section for all samples was W14 × 398 with a nominal yield stress (σ_{yn}) of 345 MPa and 406 × 292 × 32 mm³ filler plates were welded to the flanges. The thickness of the filler plates increased the column area, because the net

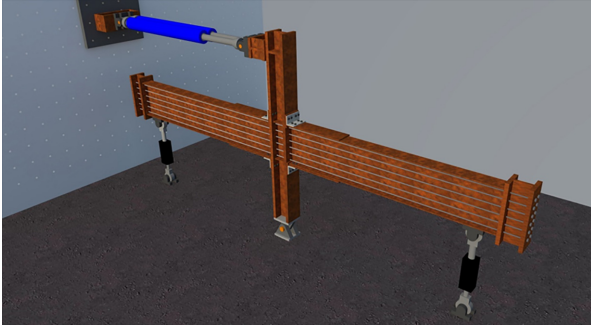


Figure 4. Configuration of specimens used by Garlock et al. (2005).

Table 1. Properties of materials (Garlock et al., 2005).

Item	σ_y (MPa)	σ_u (MPa)
Beam flange	362	498
Beam web	414	527
Reinforcing plate	397	574
Column flange	356	499
Column web	345	496
Angles	383	545
PT cables	1620	523

PT: post-tensioned.

area of the column decreased by the holes created for passing the cables. The height of the filler plate was selected in such a way that the angle, beam flange, and its fillets were in contact with the column flange. The panel zone of the column was reinforced with a 25-mm-thick continuity plate. Doubler plates used in the panel zone were designed to hold the column in an elastic state. The continuity plates were considered as the thickness of beam flanges.

The specifications of the materials used by Garlock et al. (2005) were applied for modeling the SC connection. In the study by Garlock et al. (2005), several

experiments were conducted to obtain the actual properties of materials and uniaxial tensile tests were performed in accordance with ASTM1991. Table 1 shows the static yield stress defined by Galambos (1998) as well as the ultimate stress for beam, column, angle, and continuity plates. Steel A572 was used in all specimens based on the ASTM standard with the yield and ultimate stresses of 345 and 448 MPa, respectively.

Mesh selection and contact surfaces

All members were modeled by continuous three-dimensional (3D) solid elements for FE modeling of the steel frame with SC connection. As shown in Figure 5, the specimens were meshed by 3D hexahedral element C3D8R (eight-node linear brick) with reduced integral in the ABAQUS software. A mesh study was carried out to find the mesh sizes which provide sufficient accuracy. Finer meshes were considered near the panel zone and angles, which experienced a higher variation in stress and strain. Tie constraint was used to model the interaction between the welded members. The general contact algorithm was used to model non-welded members. Tangential and normal behaviors were considered between contacting surfaces. A friction coefficient of 0.35 was considered in accordance with the AISC 360-10 (2010) guidelines. Normal behavior was applied as hard contact to prevent the penetration of the two adjacent surfaces. To obtain more accurate solutions, the whole frame was modeled disregarding the symmetry condition for the steel frame. The studies by Al Kajbaf et al. (2018) were used for FE modeling of the steel frame with an SC connection.

Boundary and loading conditions

Roller boundary conditions were considered for each beam at a distance of 4496 mm from the center of the column (displacement perpendicular to the frame plane

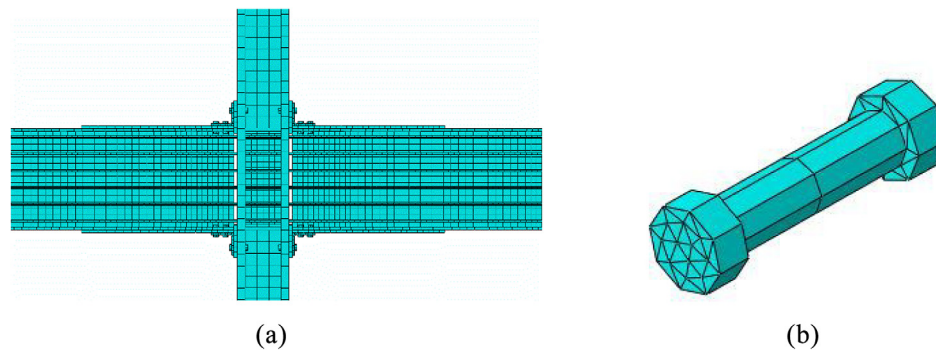


Figure 5. Meshing details of the FE model: (a) panel zone and (b) bolt.

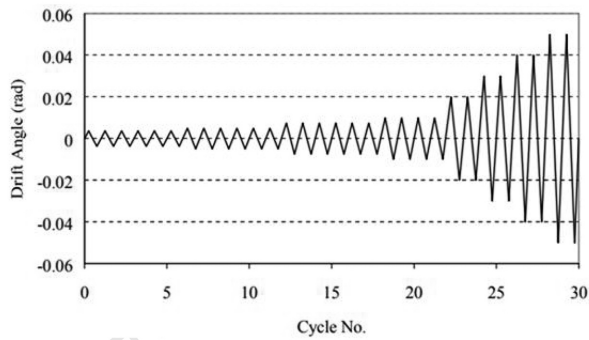


Figure 6. SAC (Venture, 1997) loading protocol.

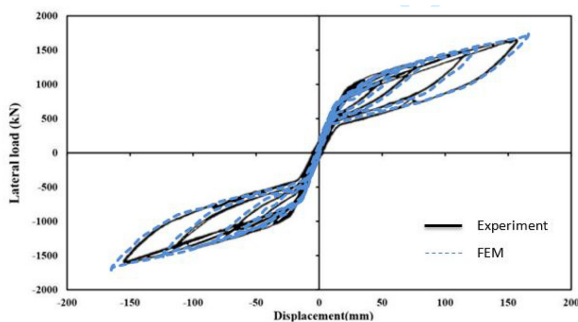


Figure 7. Hysteresis curves for analytical and laboratory specimens.

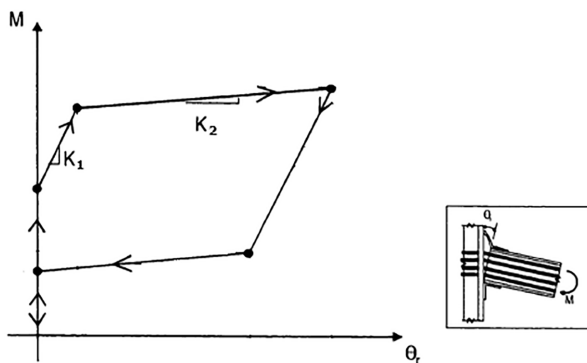


Figure 8. Simple model of moment rotation response of SC connection (Garlock et al., 2005).

was zero). Pinned boundary conditions were met at the column base, restricting its displacement in all directions while allowing its free rotation. To prevent out-of-plane displacement of beams under cyclic loading, their lateral displacements were restricted. Prestressing forces were applied to bolts and cables according to Garlock et al. (2005). In the conducted experiments, the loads were applied to the top of the column by two actuators. The loading protocol in accordance with

SAC (Venture, 1997) is shown in Figure 6. In the FE modeling of the connection, the loads are applied as displacement to a point on the top of the column flange. Each cycle is applied once to the connection to reduce the analysis time.

Verification of the FE model

To verify the ABAQUS model, the force–displacement diagrams of the specimen and the FE model were compared. Figure 7 presents the comparison of the hysteresis curves of the laboratory and analytical specimens. Specifications of the materials reported by Garlock et al. (2005) were used for model verification. As can be seen, there is a good agreement between the hysteresis curves of analytical and laboratory specimens.

FE analysis of the steel frame with SC connection under stress relaxation

Figure 8 presents a simplified graph of Figure 2. It shows the moment–relative rotation diagram of an SC connection, where θ_r is the relative rotation of the beam and the column when gap opening occurs. Before gap opening, the connection behaves as a rigid connection and θ_r is zero until the gap opens between the beam and the column. The initial stiffness of the connection after decompression is attributed to the stiffness of the angles and axial stiffness of the prestressed cables (K_1). With an increase in the moment, the angles will yield. The secondary stiffness of the connection is mostly associated with the stiffness of prestressed cables (K_2).

Stiffness of the SC connection under stress relaxation

To examine connection stiffness under stress relaxation, the FE model is considered with beam supports and pinned support at the column base on the basis of the laboratory specimen. As shown in Figure 4, monotonic loading is applied to a point on the top of the column flange in the FE model. In the first step, gravitational force is applied to the model while applying prestressing force to the cables and bolts. In the second step, the point loads are applied to the top of the column flange.

To examine the connection stiffness, the moment–rotation curves for each connection are compared in the specified prestressing ratios. The amount of debonding of the beam flange relative to the column is used to calculate the connection rotation. It can be observed from Figure 9 that diagrams are composed

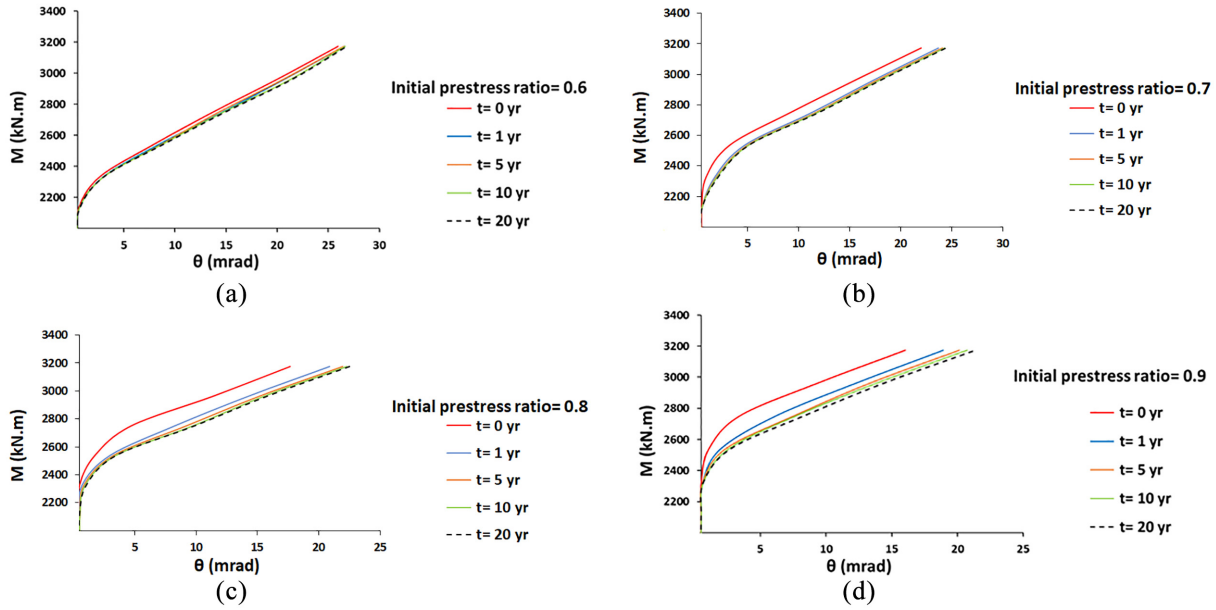


Figure 9. Moment–relative rotation curves for the SC connection at different times with the prestressing ratios of (a) 0.6, (b) 0.7, (c) 0.8, and (d) 0.9.

Table 2. SC connection stiffness at different times (kN·m/mrad).

t (years)	f_s/f_{si}			
	0.6	0.7	0.8	0.9
0	69	150	320	660
1	62	99	165	264
5	60	98	151	211
10	60	94	145	191
20	60	93	142	181

SC: self-centering.

Table 3. Ratios of SC connection stiffness at different times to the initial value.

t (years)	f_s/f_{si}			
	0.6	0.7	0.8	0.9
0	1.00	1.00	1.00	1.00
1	0.90	0.66	0.52	0.40
5	0.87	0.65	0.47	0.32
10	0.87	0.63	0.45	0.29
20	0.87	0.62	0.44	0.27

SC: self-centering.

of two regions with different slopes after debonding of the beam from the column, as in Figure 8. In the first region of the diagrams, the stiffness of the connection comprises the stiffness of the angles and the axial stiffness of the prestressed cables, which is reduced under

the stress relaxation effect on the cables. Reducing the stress of cables affects the performance of the angles, but it does not create any impact on the axial stiffness of cables. That is why in the second region of the diagrams, depicted in Figure 9, where the stiffness is due to the axial stiffness of the cables, the slope of the diagrams is the same at different times. The stiffness of the connection (K_1) in different ratios of prestressing and different times is calculated and presented in Table 2. Considering the fifth year as the basis of comparison, the connection stiffness decreases by 12%, 35%, 53%, and 68% at the prestressing ratios of 0.6, 0.7, 0.8, and 0.9, respectively, compared to the initial value (at $t = 0$).

The stiffness at the specified times relative to the initial value reported in Table 3 is displayed on the vertical axis in Figure 10. Equation (2) can be presented to estimate the reduction in the stiffness of the connection

$$\frac{K_t}{K_0} = 1 - 0.41 \times \log t \left(\frac{f_{si}}{f_y} - 0.55 \right) \quad (2)$$

where K_0 is the initial stiffness of the connection, t is the time in hours, and K_t is the stiffness of the SC connection at time t after prestressing.

SC connection under stress relaxation in cyclic loading

To examine the moment–rotation diagram of the SC connection under cyclic loading and stress relaxation,

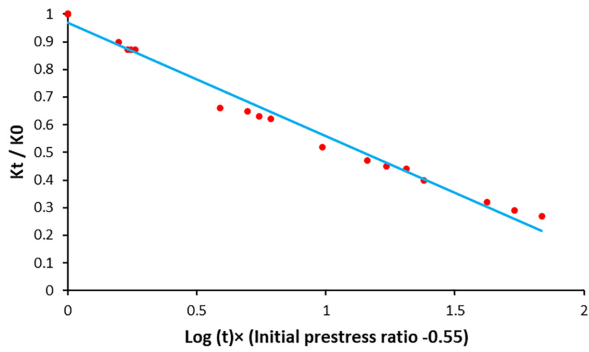


Figure 10. Reduction in SC connection stiffness under stress relaxation.

the FE model is considered with beam supports and pinned support at the column base on the basis of the laboratory specimen. As shown in Figure 4, the loads in the FE model are applied as displacement to a point on the top of the column flange according to the loading protocol presented in Figure 6. To reduce the analysis time, each cycle is applied once to the connection. To study the cyclic behavior of the connection under stress relaxation, the moment–rotation hysteresis and backbone diagrams of each connection are compared at specified prestressing ratios. The amount of debonding of the flange of the beam relative to the column is used to calculate the connection rotation. As shown in Figures 11 to 14, stress relaxation leads to reduced

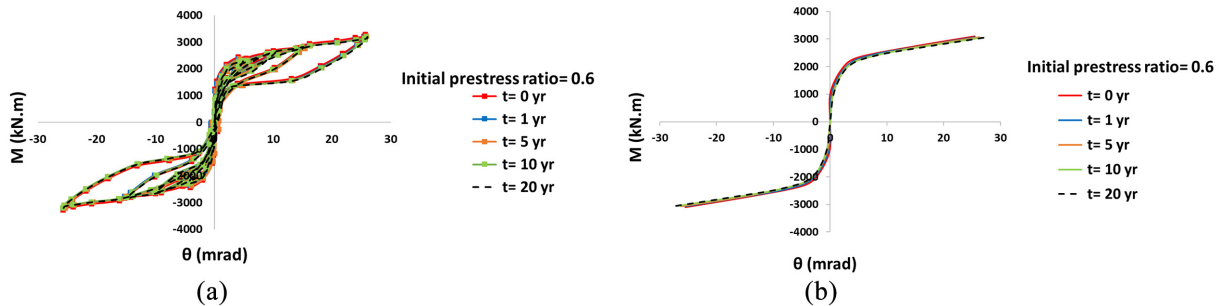


Figure 11. Diagrams of the SC connection versus time at a prestressing ratio of 0.6: (a) hysteresis curves and (b) backbone curves.

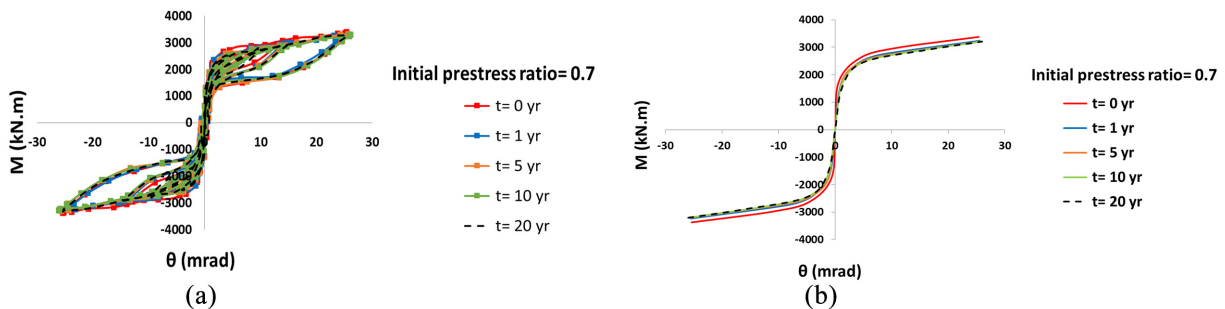


Figure 12. Diagrams of SC connection versus time at a prestressing ratio of 0.7: (a) hysteresis curves and (b) backbone curves.

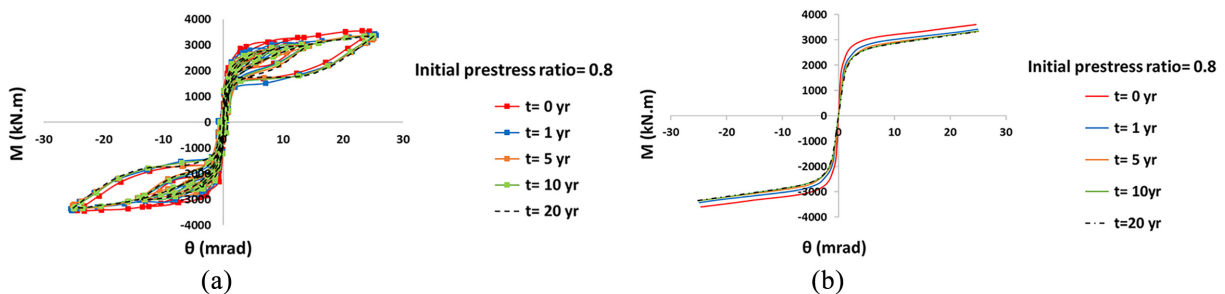


Figure 13. Diagrams of SC connection versus time at a prestressing ratio of 0.8: (a) hysteresis curves and (b) backbone curves.

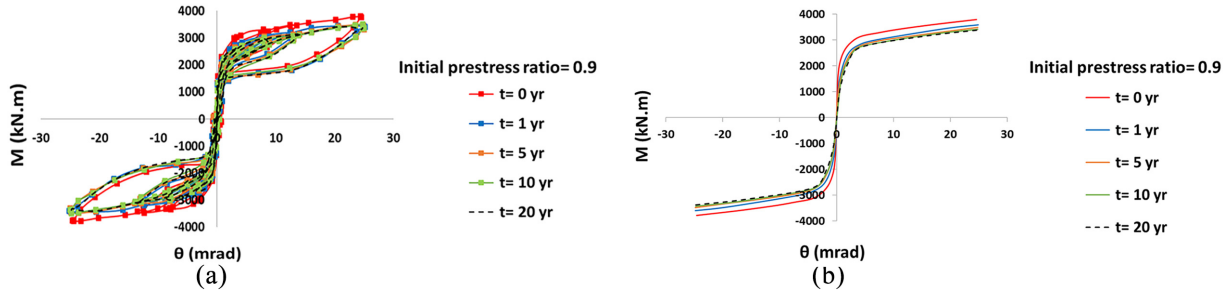


Figure 14. Diagrams of SC connection versus time at a prestressing ratio of 0.9: (a) hysteresis curves and (b) backbone curves.

Table 4. Dissipated energy by the system at different times (kJ).

t (years)	f_d/f_i			
	0.6	0.7	0.8	0.9
0	118.8	126.0	136.5	148.5
1	117.6	122.0	129.7	136.1
5	117.2	121.0	126.3	133.1
10	117.2	120.0	125.8	132.7
20	117.2	119.9	124.1	130.0

Table 5. Ratio of dissipated energy by the system at different times to the initial value.

t (years)	f_s/f_{si}			
	0.6	0.7	0.8	0.9
0	1.00	1.00	1.00	1.00
1	0.99	0.97	0.95	0.92
5	0.99	0.96	0.92	0.90
10	0.99	0.95	0.92	0.89
20	0.99	0.95	0.91	0.88

dissipated energy by the system so that more energy is dissipated with an increase in the prestressing ratio. The stress change in the cables is effective in the first region and it does not exert any impact on the stiffness of the connection in the second region of Figure 8. A reduction in dissipated energy by the system is lower than that in connection stiffness in the first region due to the stress relaxation phenomenon.

The dissipated energy at different ratios of prestressing and different times is calculated and presented in Table 4. Considering the fifth year as the basis of comparison, the dissipated energy is reduced by 1%, 4%, 8%, and 10% at the prestressing ratios of 0.6, 0.7, 0.8, and 0.9, respectively, compared to the initial value (at $t = 0$). The ratio of dissipated energy at specified times to the initial dissipated energy reported in Table 5 is

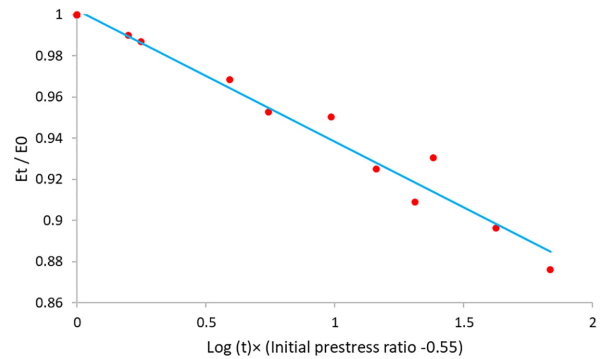


Figure 15. Reduction in dissipated energy by the SC moment frame under stress relaxation.

displayed on the vertical axis in Figure 15. Equation (3) can be presented to estimate the reduction in dissipated energy by the system

$$\frac{E_t}{E_0} = 1 - 0.064 \times \log t \left(\frac{f_{si}}{f_y} - 0.55 \right) \quad (3)$$

where E_0 is the initial dissipated energy, t is the time in hours, and E_t is the dissipated energy by the system at time t after prestressing.

Conclusion

To investigate the effect of stress relaxation on the performance of a steel frame with SC connection, the laboratory models developed by Garlock et al. (2005) were studied at the prestressing ratios of 0.6, 0.7, 0.8, and 0.9. A model with monotonic loading was used to study the connection stiffness. A model under cyclic loading was also used for evaluating the cyclic behavior and dissipated energy by the SC connection. The main results are summarized as follows:

1. The changes in stiffness and dissipated energy by the steel frame with SC connection were much higher in the first 10 years than in the

second 10 years. One can conclude the relatively good stability of the connection in the second 10 years.

2. At a prestressing ratio of 0.6, the stiffness and dissipated energy by the SC connection were not affected by stress relaxation over time; thus, the connection showed a stable behavior throughout the life of the structure. The system showed higher stiffness and dissipated energy at larger prestressing ratios.
3. Considering the fifth year as the basis of comparison, stiffness was reduced by 12%, 35%, 53%, and 69% at the prestressing ratios of 0.6, 0.7, 0.8, and 0.9, respectively, compared to the initial value.
4. Considering the fifth year as the basis of comparison, dissipated energy was reduced by 1%, 4%, 8%, and 10% at the prestressing ratios of 0.6, 0.7, 0.8, and 0.9, respectively, compared to the initial value.
5. Considering the changes in the stiffness of the SC connection at different prestressing ratios under stress relaxation, equation (2) was presented to predict stiffness reduction.
6. Given the changes in the energy dissipated by SC-MRF at different prestressing ratios under stress relaxation, equation (3) was presented to predict the reduction in dissipated energy by the system.

In this study, the effect of stress relaxation on the performance of an SC connection with bolted top-and-seat angles as energy dissipater devices is investigated. For future studies, the effect of stress relaxation on the performance of an SC connection with dampers can be investigated.


Declaration of Conflicting Interests

The author(s) declared no potential conflicts of interest with respect to the research, authorship, and/or publication of this article.

Funding

The author(s) received no financial support for the research, authorship, and/or publication of this article.

ORCID iD

Nader Fanaie  <https://orcid.org/0000-0002-6789-8930>

References

ABAQUS/PRE (2011) *User Manual, V6.14*. Providence, RI: Hibbit, Karlsson & Sorensen.

- AISC 360-10 (2010) Specification for structural steel buildings.
- Al Kajbaf A, Fanaie N and Faraji Najarkolaie K (2018) Numerical simulation of failure in steel posttensioned connections under cyclic loading. *Engineering Failure Analysis* 91: 35–57.
- Atienza JM and Elices M (2007) Role of residual stresses in stress relaxation of prestressed concrete wires. *Journal of Materials in Civil Engineering* 19: 703–708.
- Au FT and Si X (2012) Time-dependent effects on dynamic properties of cable-stayed bridges. *Journal of Structural Engineering and Mechanics* 41: 139–155.
- Dong H, Du X and Han Q (2019) Seismic responses of steel frame structures with self-centering energy dissipation braced on shape memory alloy cables. *Journal of Advances in Structural Engineering* 22: 2136–2148.
- Engelhardt MD and Sabol TA (1998) Reinforcing of steel moment connections with cover plates: benefits and limitations. *Engineering Structures* 20: 510–520.
- Filiatrault A, Restrepo J and Christopoulos C (2004) Development of self-centering earthquake resisting systems. In: *Proceedings of the 13th world conference on earthquake engineering*, Vancouver, BC, Canada, 1–6 August.
- Findley WN, Lai JS and Onaran K (1976) *Creep and Relaxation of Nonlinear Viscoelastic Materials*. Amsterdam: North Holland Publishing Company.
- Galambos TV (1998) *Guide to Stability Design Criteria for Metal Structures*. Hoboken, NJ: John Wiley & Sons.
- Garlock MM, Ricles JM and Sause R (2005) Experimental studies of full-scale posttensioned steel connections. *Journal of Structural Engineering* 131: 438–448.
- Guan X, Burtona H and Moradi S (2018) Seismic performance of a self-centering steel moment frame building: from component-level modeling to economic loss assessment. *Journal of Constructional Steel Research* 150: 129–140.
- Huang L, Zhou Z, Zhang Z, et al. (2018) Seismic performance and fragility analyses of self-centering prestressed concrete frames with infill walls. *Journal of Earthquake Engineering*. Epub ahead of print 11 February. DOI: 10.1080/13632469.2018.1526142.
- Lafortune P, McCormick J, Desroches R, et al. (2007) Testing of superelastic recentering pre-strained braces for seismic resistant design. *Journal of Earthquake Engineering* 11: 383–399.
- Magura DD, Sozen MS, Siess CP, et al. (1964) A study of stress relaxation in prestressing reinforcements. *Journal of the Prestressed Concrete Institute* 9: 13–57.
- Miller DK (1998) Lessons learned from the Northridge earthquake. *Engineering Structures* 20: 249–260.
- Nakashima M, Inoue K and Tada M (1998) Classification of damage to steel buildings observed in the 1995 Hyogoken-Nambu earthquake. *Engineering Structures* 20: 271–281.
- Smith T, Ponzo FC, Di Cesare A, et al. (2014) Post-tensioned glulam beam-column joints with advanced damping systems: testing and numerical analysis. *Journal of Earthquake Engineering* 18: 147–167.
- Sreevalli IY and Rao GA (2010) Prediction of time dependent effects in prestressed concrete. In: *Proceedings of FraMCoS-7*, 23–28 May, pp.755–759.

- Tremblay R and Filiatrault A (1997) Seismic performance of steel moment resisting frames retrofitted with a locally reduced beam section connection. *Canadian Journal of Civil Engineering* 24: 78–89.
- Trevino J and Ghali A (1985) Relaxation of steel in prestressed concrete. *PCI Journal* 30: 82–94.
- Tzimas AS, Dimopoulos AI and Karavasilis TL (2015) EC8-based seismic design and assessment of self-centering post-tensioned steel frames with viscous dampers. *Journal of Constructional Steel Research* 105: 60–73.
- Venture SJ (1997) *Protocol for fabrication, inspection, testing, and documentation of beam-column connection tests and other experimental specimens*. Rep. No. SAC/BD-97.
- Xian X, Yanfeng Z and Yaozhi L (2107) Self-centering links using post-tensioned composite tendons. *Journal of Advances in Structural Engineering* 21: 1302–1312.
- Zeren A and Zeren M (2003) Stress relaxation properties of prestressed steel wires. *Journal of Materials Processing Technology* 141: 86–92.